Photochemistry and Photobiology, 20**, **: *–*

Analysis and Design of Photobioreactors for Microalgae Production I: Method and Parameters for Radiation Field Simulation

Josué Miguel Heinrich[1,2], Ignacio Niizawa[1], Fausto Adrián Botta[1,2], Alejandro Raúl Trombert[2] and Horacio Antonio Irazoqui*[1,2]

[1]Group of Innovation on Bio-processes Engineering, Institute for the Technological Development of the Chemical Industry (INTEC), National Research Council (CONICET) and University of Litoral (UNL), Santa Fe, Argentina

[2]Group of Innovation on Bio-processes Engineering, Department of Biochemistry and Biological Sciences (FBCB), University of Litoral (UNL), Ciudad Universitaria, Santa Fe, Argentina

Received 20 December 2011, accepted 4 March 2012, DOI: 10.1111/j.1751-1097.2012.01141.x

ABSTRACT

Having capabilities for the simulation of the radiation field in suspensions of microalgae constitutes a great asset for the analysis, optimization and scaling-up of photobioreactors. In this study, a combined experimental and computational procedure is presented, specifically devised for the assessment of the coefficients of absorption and scattering, needed for the simulation of such fields. The experimental procedure consists in measuring the radiant energy transmitted through samples of suspensions of microalgae of different biomass concentrations, as well as the forward and backward scattered light. At a microscopic level, suspensions of microalgae are complex heterogeneous media and due to this complexity, in this study they are modeled as a pseudocontinuum, with centers of absorption and scattering randomly distributed throughout its volume. This model was tested on suspensions of two algal species of dissimilar cell shapes: *Chlorella sp*. and *Scenedesmus quadricauda*. The Monte Carlo simulation algorithm developed in this study, when used as a supporting subroutine of a main optimization program based on a genetic algorithm, permits the assessment of the physical parameters of the radiation field model. The Monte Carlo algorithm simulates the experiments, reproducing the events that photons can undergo while they propagate through culture samples or at its physical boundaries.

INTRODUCTION

Microalgae are highly valuable microorganisms because they are the light harvesting ''cell factories'' that convert carbon dioxide into biomass or a variety of bioactive compounds (1). They are used in such diverse areas as oil source for biofuel production, food manufacturing, cosmetics and pharmaceuticals industries; and as a means for wastewater treatment in bioremediation (2–9).

The mass production of microalgae can be carried out in either open or closed systems. In open systems, microalgae are grown in large land areas with minimal care regarding weather conditions and contamination risks (1,10). On the other hand, closed photobioreactors (PBRs) make possible the efficient control of the culture variables, such as pH, temperature, concentration of carbon dioxide in the air streams fed to algal suspensions, etc.; as well as a better contamination prevention (1,11).

Light is the only source of energy in photoautotrophic microorganisms' growth. Therefore, one of the major concerns in microalgae production is achieving an efficient use of light in the culture. A suitable design of a PBR necessarily includes intrinsic growth kinetics, specific to each photosynthetic microorganism, which must be related to the suitable property of the light field at each position throughout the volume of the algal culture (12,13). Typical submerged cultures of microalgae are nonhomogeneous suspensions, which consist in a cloud of algal cells dispersed throughout the volume of a saline solution. A bubbling gas stream (usually atmospheric air) is used as a means to deliver CO_2 to the medium and to stir the suspension. If the culture medium is transparent to visible light, every beam of light can be either absorbed or scattered while it travels through the culture, only if one of these obstacles is found along its trajectory.

In several studies, physical and mathematical models of light transfer have been proposed for the analysis, simulation, design, scale-up and optimization of PBRs (14). These approaches are based on the Beer–Lambert law (15,16), the two-fluxes approximation (17–19) and on discrete ordinate methods (20). Although it is always a difficult task, the solution of the radiative transfer equation (RTE) for the system under study gives the spatial and directional distribution of radiation intensities (21).

To solve the RTE inside PBRs the spectral radiative properties (volumetric absorption coefficient α_λ, volumetric scattering coefficient ξ_λ, and parameters of the models chosen for the scattering phase function $B(\underline{\hat{\Omega}}' \cdot \underline{\hat{\Omega}})$) of the culture suspension are required. These properties can be estimated either with experimental methods (22,23) or with theoretical approaches (*i.e.* by Mie theory; 24).

Numerous experimental investigations have been performed to study the scattering of electromagnetic waves. A comprehensive review of the experimental techniques for measuring radiation field properties has been published by Agrawal and

*Corresponding author email: hirazo@santafe-conicet.gov.ar (Horacio A. Irazoqui)

Mengüc (25). One of those methods consists of determining the extinction coefficient β_λ by measuring the normal–normal transmittance (26,27). Another practice is the use of an integrating sphere.

The methodology used in this study implies measuring the radiant energy transmitted through samples of different microalgal suspensions, as well as the scattered light in the forward and backward directions using an integrating sphere. The mutually independent experimental measurements carried out in this study are: the monochromatic direct transmittance; the monochromatic diffuse transmittance and reflectance.

The experimental measurements were performed within the wavelength range from 400 to 700 nm, corresponding to the radiation useful for photosynthesis (28,29).

The values of α_λ, ξ_λ, as well as those of the parameters of the mathematical model chosen for the scattering phase function were not directly measured in this set of experiments. Instead, they were obtained as the set of values that result in the ''best fit'' between experimental results and those predicted by the simulation of the experimental measurements using a specifically devised stochastic algorithm, based on the Monte Carlo method (30–32).

The effectiveness of the methodology was proven on suspensions of two different algal species: *Chlorella* sp. and *Scenedesmus quadricauda*. With the optical parameters correlated with different algal concentrations, the Monte Carlo simulator can be used as an autonomous predictive tool for PBRs design, simulation and optimization purposes. The advantage in using a Monte Carlo based simulation module relies on the fact that, by ''mimicking'' the path of photons throughout the PBR, it is possible to reproduce with accuracy the radiation field in the culture medium, considering the geometry and boundaries of the reactors, the presence of bubbles, and the characteristics of the light emitting systems (emission properties, configuration, etc.).

MATERIALS AND METHODS

Algal strains and culture medium. Two algal strains were used as model microorganisms: *S. quadricauda* (from Culture Collection of Algae and Protozoa, UK) and *Chlorella* sp. (kindly provided by Dr. A.M. Gagneten, FHUC and UNL). Cylindrical cells of *S. quadricauda* are assembled in planar clusters of up to four parallel units, while *Chlorella* sp. resembles ellipsoids revolving about their major axis (Fig. 1). These algae strains were chosen due to their different shapes, thus opening the possibility of experimentally assessing the impact of the shape of the model microorganism on the scattering properties of an algal suspension.

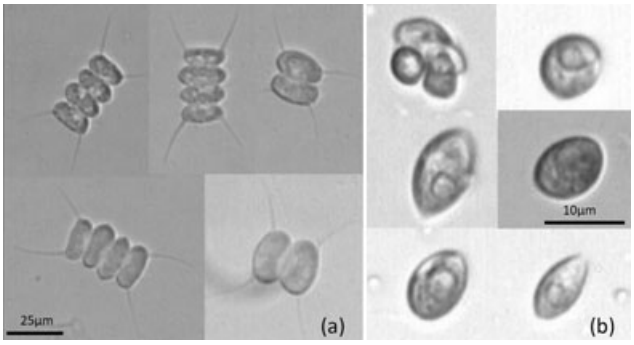

Figure 1. Micrographs of the two microalgal species used in this work: (a) *Scenedesmus quadricauda* and (b) *Chlorella* sp. Scale.

Batch cultures of each of the microalgae strains were conducted under similar conditions. Each of several Erlenmeyer flasks, partially filled with equal volumes of sterilized BG-11 (33) culture medium (750 mL each) was inoculated with a single isolated algal species. Each strain was axenically grown exposed to artificial light from a daylight lamp (20 W Philips). The culture medium is totally transparent to radiant energy within the 400–700 nm wavelength range.

The suspension was well mixed by a bubbling atmospheric air stream, previously sterilized by flowing through a 0.45 μm pore size filter. The air stream also supplies the culturing flasks with the necessary CO_2 and strips out the O_2 generated by oxygenic photosynthesis. The operation was continued until a sufficiently high-biomass concentration was reached (typically 1.0 g L^{-1}).

The preparation of reference suspensions and measurement of biomass concentration. The algal cells suspended in an aliquot volume of the original culture were separated by centrifugation and then suspended again in the volume of fresh medium just needed to obtain a more concentrated reference suspension. The algal mass concentration of this initial reference suspension was determined by measuring the dry weight (DW) of the total suspended solids (TSS; 34). The algal mass contained in a 50 mL sample was retained by a 0.45 μm pore diameter filter, and then washed with 30 mL of distilled water and dried at 100°C for 60 min. The DW of solids suspended in the concentrated reference suspension was calculated as the difference between the DW of the clean filter and that of the filter with the retained solids. The algal mass concentration was reported as the DW of suspended solids per unit volume of the sample. From aliquots of the concentrated reference suspension, diluted samples were prepared of 1/5, 2/25 and 1/25 dilution ratios.

The measurement of the specific chlorophyll content of the reference suspensions. The total chlorophyll content of the reference suspensions was determined by the method reported by Ritchie (35). Aliquots of the samples were centrifuged to collect the suspended cells. The cells were washed with distilled water and centrifuged once again. The harvested cells were suspended in methyl alcohol and the chlorophylls were extracted by heating the methylic suspension at 80°C for 5 min. The chlorophyll content was calculated from the values of the light absorbance at wavelengths of 632, 652 and 665 nm, using the absorbance coefficients reported in the article quoted elsewhere. The biomass and chlorophyll concentrations of the prepared reference suspensions are summarized in Table 1.

Measurement of direct transmittance, diffuse reflectance and transmittance. Three complementary and mutually independent experiments were carried out to measure the monochromatic direct transmittance, the spectral diffuse transmittance and the spectral diffuse reflectance on algae suspensions of different concentration of biomass. Although the experimental setup is the same to that used by Satuf *et al*. (36) for metallic oxide suspensions, the results were processed in an entirely different manner.

Measurements were made first on the sterile culture medium, and then on the prepared algal suspensions of different concentration (DW), contained in a polystyrene cuvette of $10 \times 10 \times 40$ mm. Spectrophotometric readings were made within the visible region of the electromagnetic spectrum, with wavelengths ranging from 400 to 700 nm.

The spectral direct transmittance was measured with an Optronic OL series 750 spectrophotometer (Optronic Laboratories, Inc., Orlando, FL) with the sample placed between the radiation source and the detector (Fig. 2a). The detector used in this experiment has a large angle of acceptance and no precaution was taken to eliminate the scattered light or to ensure the prevalence of simple scattering, in contrast to what is usually done in normal–normal transmittance measurements.

Table 1. Preparation of microalgae suspensions from algal cultures. Biomass concentration and chlorophyll content of reference suspensions.

Algal species	*Chlorella* sp.	*Scenedesmus quadricauda*
Biomass DW concentration [g L^{-1}]	1.650	1.355
Chlorophyll [mg gDW^{-1}]	47.4	57.8

DW, measurement of biomass dry weight.

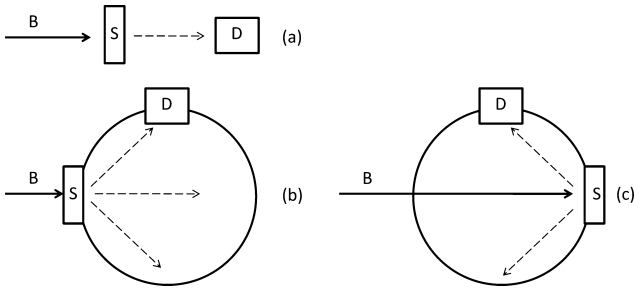

Figure 2. Schematic representation of the configurations of the detector for the optical properties measurements. (a) Direct transmittance; (b) diffuse transmittance and (c) diffuse reflectance. S, sample, D, detector, AA, detector acceptance angle and B, collimated monochromatic beam.

The measurements of diffuse transmittance and reflectance were performed using an OL 740–70 integrating sphere attachment, assembled as it is schematically shown in Fig. 1b,c, as it is required by each experiment. The internal wall of integrating sphere is coated with poly-tetrafluoroethylene (PTFE) to ensure diffuse total reflection and the detector is positioned on a port mounted on top of the sphere. The design of the integrating sphere includes internal baffles, also coated with PTFE, conveniently placed to avoid the possibility that light may directly reach the detector, thus ensuring that only indirect (or reflected) energy beams are recorded.

Simulation method. Physical and mathematical model of light transfer: As it was previously mentioned, physical and mathematical models of light transfer have been proposed for the analysis, simulation, design, scale-up and optimization of PBRs (14–20). Approaches based on Beer–Lambert law predict the energy loss experienced by a light beam while passing through an algal suspension, accounting for both absorption and out-scattering, but disregards in-scattering contributions, which could lead to errors when predicting the light intensity profile in PBRs (14). The two-flux approximation and the discrete ordinate methods avoid this problem by including in-scattering contributions in the solution of the RTE (14,21).

The RTE (Eq. [1]) accounts for the factors that bring about changes in the local monochromatic radiation intensity $L_{\lambda,\underline{\hat{\Omega}}}$ of a radiation beam in a participative medium like the previously described microalgal suspension; including radiation absorption; ''out-scattering'' (*i.e.* loss of radiant energy from the beam by dispersion); and ''in-scattering'' (increase of the energy of the beam due to contributions of dispersed radiant energy from other beams).

$$\underline{\hat{\Omega}} \cdot \underline{\nabla} L_{\lambda,\underline{\hat{\Omega}}}(\underline{r},t) + [\alpha_\lambda(\underline{r},t) + \xi_\lambda(\underline{r},t)] L_{\lambda,\underline{\hat{\Omega}}}(\underline{r},t) = \frac{\xi_\lambda}{4\pi} \int_{\underline{\hat{\Omega}}'} \mathrm{d}^{(2)}\underline{\hat{\Omega}}' B\left(\underline{\hat{\Omega}}' \cdot \underline{\hat{\Omega}}\right) L_{\lambda,\underline{\hat{\Omega}}'}(\underline{r},t) \quad (1)$$

In Eq. (1), $\alpha_\lambda(\underline{r},t)$ is the local volumetric absorption coefficient; $\xi_\lambda(\underline{r},t)$ is the local volumetric scattering coefficient and $B\left(\underline{\hat{\Omega}}' \cdot \underline{\hat{\Omega}}\right)$ is the scattering phase function. For our purposes, the latter can be thought of as the conditional probability distribution that a photon, which travels in the $\underline{\hat{\Omega}}$ direction is deflected into the $\underline{\hat{\Omega}}'$ direction. The scattering phase function satisfies the normalization condition

$$\frac{1}{4\pi} \int_{\underline{\hat{\Omega}}} \mathrm{d}^{(2)}\underline{\hat{\Omega}}' B\left(\underline{\hat{\Omega}}' \cdot \underline{\hat{\Omega}}\right) = \frac{1}{4\pi} \int_0^{2\pi} \mathrm{d}\phi' \int_{-1}^{1} \mathrm{d}\mu_0 B(\mu_0) = \frac{1}{2} \int_{-1}^{1} \mathrm{d}\mu_0 B(\mu_0) = 1 \quad (2)$$

where $\mu_0 = \left(\underline{\hat{\Omega}}' \cdot \underline{\hat{\Omega}}\right)$.

The spectral radiative properties ($\alpha_\lambda(\underline{r},t)$, $\xi_\lambda(\underline{r},t)$ and $B(\mu_0)$) of the culture suspension are required to solve the RTE inside PBRs. Theoretical approaches are often based on the assumption that the scattering centers are particles of relatively simple shapes (*e.g.* spherical), each one acting as an independent scattering center in a medium in which single scattering prevails. In contrast, cells of microalgae are complex particles, consisting of a cell membrane surrounding the nucleus, vesicles, mitochondria, chloroplasts, ribosomes, cytoskeleton and other cellular components, such as lipids, macromolecules and starch grains, each having their own size, and different radiative properties. Moreover, some of them have a cell wall around the outside of the cell membrane. Besides, the relative amounts of cellular components, their properties and the cells size change during the different phases of the cell cycle and depend on its physiological state. The complexity of the interaction of the radiative energy field with suspensions of microalgae transcends the mere shape of the cell as well as its possible characterization as made of a uniform material with rather specific and well-characterized dielectric properties, and entails issues as the presence of particles inside particles and a nonuniform refraction index. Because no adequate theory has yet been proposed to predict scattering of radiation in such complex situations, experimental approaches are the only means to determine the radiation scattering in microalgal culture suspensions (14).

As it was previously mentioned, numerous experimental investigations have been performed to study the scattering of electromagnetic waves (25,26). The determination of the extinction coefficient β_λ by measuring the normal–normal transmittance (26) requires very dilute microalgal suspensions to ensure that simple scattering prevails. Because the light beam has a finite diameter and the detector a finite acceptance angle, care must be taken to ensure elimination of all scattered radiation that could reach the detector, otherwise several corrections will be necessary (14).

Another common practice is the use of an integrating sphere (Fig. 3a). Suspensions of microorganisms scatter light strongly in the forward direction and so a significant fraction of the scattered radiation is collected by the integrating sphere; then, the light attenuation is attributed solely to the light absorption and the absorption coefficient α_λ could be directly determined. Despite the fact that this is a technique simple to implement, the absorption coefficient obtained suffers from errors due to light scattering and various correction methods should be applied (14,26,27). When

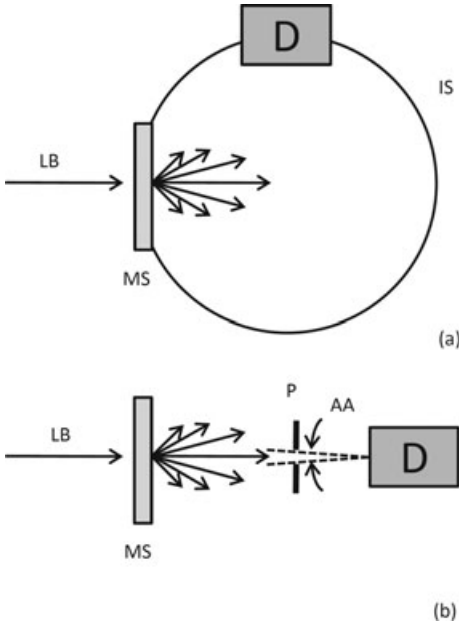

Figure 3. Experimental setup for directly determining (a) absorption coefficient α_λ from hemispherical transmittance and (b) the extinction coefficient β_λ from normal–normal transmittance. D, detector; MS, slim section of diluted microalgal suspension; AA, detector acceptance angle; P, pinhole; LB, incident light beam; IS, integrating sphere.

measured in ideal conditions, from these two experiments, the scattering coefficient can be directly determined from the equality $\beta_\lambda = \alpha_\lambda + \xi_\lambda$.

The methodology used in this study implies measuring the radiant energy transmitted through samples of different microalgal suspensions, as well as the scattered light in the forward and backward directions using an integrating sphere. Any assumption regarding ideal behavior has been avoided with the objective of obtaining the radiation field parameters from experimental measurements carried out under the same conditions encountered in large-scale microalgal mass production.

As it was previously mentioned, the measurements were performed within the wavelength range from 400 to 700 nm, disregarding the rest of the electromagnetic spectrum, because of our interest consists in modeling the field of the radiative energy that serves as a ''substrate'' for microalgal growth.

In this study, a stochastic algorithm based on the Monte Carlo method (30) is devised for the simulation of the radiation field in the algal suspensions and to reproduce the results of the experimental procedure. In such an algorithm, the algal suspension is modeled as a continuum, where the particles have lost their identity, and have been replaced either by centers of absorption or scattering, randomly distributed throughout the suspension. The Monte Carlo method requires knowing the parameters (α_λ, ξ_λ and $B(\mu_0)$) necessary to simulate the interaction between the radiative field and the suspension so as to assign a probability to each of the events that photons can undergo while traveling across the culture. To assess these properties through the simulation of the experiments performed, the Monte Carlo simulation module was used as an external subroutine of an optimization program based on a Genetic Algorithm (37,38), as will be discussed in forthcoming sections.

The scattering coefficient was correlated with the mass concentration of algae in the suspension, and it was experimentally demonstrated that it is independent of the algae size and of their shape, at least within the range of concentrations usually found in PBRs. The actual objects that cause light dispersion are the cellular components, which are present in a variety of sizes and shapes and in different relative proportions. The scattering phase function was expressed as a truncated series of Legendre polynomials.

Monte Carlo simulation of the algal suspension: The algal suspension was modeled as a continuum where the suspended cells have been replaced either by centers of absorption or of scattering, distributed randomly throughout the suspension. The Monte Carlo simulation of the radiative field in the liquid phase consists of the following steps, as sketched in Fig. 4:

Step 1: For a given set of values of λ, α_λ, ξ_λ and Δs, compute $P(\mathrm{A})$, $P(\mathrm{S})$ and $P(\mathrm{NA, NS}) = P(\mathrm{NA, NS})$ from Eqs. (3–5) (see Appendix). These values remain unchanged as long as those of λ, α_λ, ξ_λ and Δs remain the same.

$$P(\mathrm{A}) = \frac{n_{\mathrm{p}}^{(\mathrm{abs})}\left(s+\Delta s, \underline{\hat{\Omega}}, \lambda\right)}{n_{\mathrm{p}}\left(s, \underline{\hat{\Omega}}, \lambda\right)} = \frac{\alpha_\lambda}{(\alpha_\lambda + \xi_\lambda)}\{1 - \exp[-(\alpha_\lambda + \xi_\lambda)\Delta s]\} \tag{3}$$

$$P(\mathrm{S}) = \frac{\xi_\lambda}{(\alpha_\lambda + \xi_\lambda)}\{1 - \exp[-(\alpha_\lambda + \xi_\lambda)\Delta s]\} \tag{4}$$

$$P(\mathrm{NA, NS}) = \exp\{-(\alpha_\lambda + \xi_\lambda)\Delta s\} = 1 - P(\mathrm{S}) - P(\mathrm{A}) \tag{5}$$

Step 2: Choose an initial position $\underline{r}_0$ on the illuminated sector of the light entrance boundary of the cuvette containing the algal suspension. Choose an initial direction of motion $\underline{\hat{\Omega}}_0(\phi_0, \mu_0)$ for an entering (λ) photon. Move the photon a distance Δs from its initial position $\underline{r}_0$ in its $\underline{\hat{\Omega}}_0$ initial direction to reach a position $\underline{r}_0 + \underline{\hat{\Omega}}_0 \Delta s$ in the suspension, but still very close to the light entrance boundary.

Step 3: At every stage of the computation, take a Δs step forward from the current photon position $\underline{r}$ in the current photon direction $\underline{\hat{\Omega}}$, to pinpoint a new $\underline{r}' = \underline{r} + \underline{\hat{\Omega}}\,\Delta s$ position that the photon might reach.

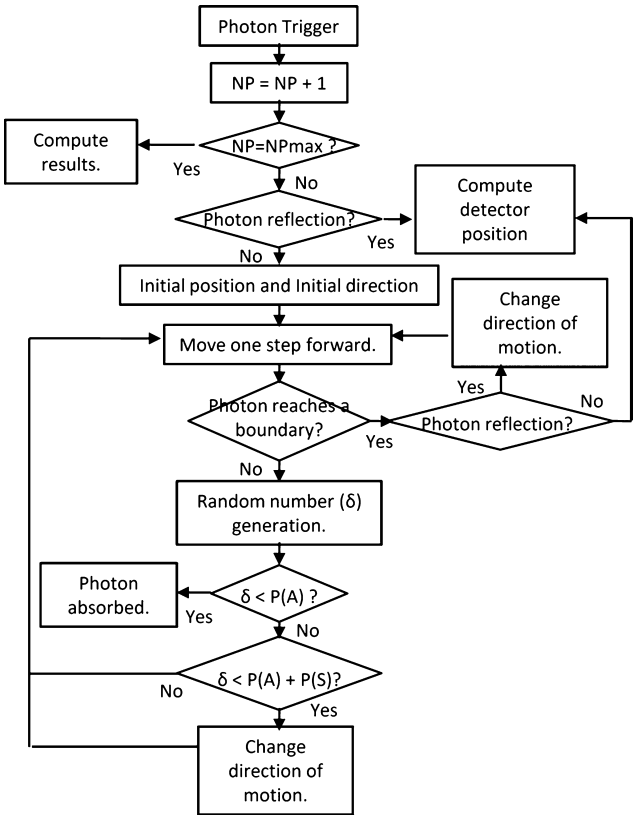

Figure 4. Schematic representation of the Monte Carlo algorithm employed for the simulation of the radiant energy field in the algal suspension.

If this were the first photon move after Step 2, the current photon position would be $\underline{r}_0$; the corresponding direction of motion $\underline{\hat{\Omega}}_0$; and the new position $\underline{r}' = \underline{r}_0 + \underline{\hat{\Omega}}_0\,\Delta s$.

Step 4: On the basis of the values of $P(\mathrm{A})$, $P(\mathrm{S})$ and $P(\mathrm{NA, NS})$ from Step 1, the problem we have to deal with now is to establish which event among absorption (event A), scattering (event S) and their complementary compound event (NA, NS) will occur to the photon as it moves in the direction $\underline{\hat{\Omega}}$ from the position $\underline{r}$ toward the new position $\underline{r}'$. For this, a random number δ, ($0 \le \delta \le 1$), is generated and check whether $0 \le \delta \le P(\mathrm{A})$, $P(\mathrm{A}) \le \delta \le P(\mathrm{A}) + P(\mathrm{S})$ or $P(\mathrm{A}) + P(\mathrm{S}) \le \delta \le 1$.

If $0 \le \delta \le P(\mathrm{A})$, the photon is assumed to have been absorbed. We increase by one the absorbed photons counter at the position $\underline{r}'$ and a new photon has to be fired, regaining the computation scheme at Step 1.

If $P(\mathrm{A}) \le \delta \le P(\mathrm{A}) + P(\mathrm{S})$, then the photon at point $\underline{r}'$ is assumed to have been deflected from its original direction of motion $\underline{\hat{\Omega}}$ into a new $\underline{\hat{\Omega}}'$ direction. The likelihood of a $\underline{\hat{\Omega}} \to \underline{\hat{\Omega}}'$ transition depends on the ''dot'' product $(\underline{\hat{\Omega}} \cdot \underline{\hat{\Omega}}')$ through the scattering phase function $B(\underline{\hat{\Omega}}' \cdot \underline{\hat{\Omega}})$, which has the physical meaning of a transition probability distribution function. In the context of the Monte Carlo simulation of the radiant field in a homogeneous algal suspension, the scattering phase function is the means at our disposal to choose the new direction of motion of the deflected photon, as we shall see in the next section. With the new direction, the algorithm is restarted at Step 3.

If $P(\mathrm{A}) + P(\mathrm{S}) \le \delta \le 1$, then the photon is assumed to have preserved its direction of motion $\underline{\hat{\Omega}}$ and the algorithm is restarted from Step 3. If we follow the path of a large number of photons ''fired'' to the cuvette we can reproduce by simulation the experimental results.

When used in its simulation mode, the Monte Carlo algorithm just described requires knowing the values of the volumetric scattering and absorption coefficients of the homogeneous solution, as well as its scattering phase function, to compute the probability of each of the events, which determine the fate of a tracked photon. In this study, the Monte Carlo algorithm was first used as a supporting subroutine of an

optimization program based on a Genetic Algorithm (37,38) to regress α_λ and ξ_λ from experimental data as functions of the chlorophyll content and of the algal mass concentration of the homogeneous suspension, as well as the parameters involved in $B(\underline{\hat{\Omega}}' \cdot \underline{\hat{\Omega}})$.

The light scattering phase function and the Monte Carlo simulation of a radiant field in an algal suspension: A $(\underline{\hat{\Omega}}, \lambda)$ photon, which undergoes a scattering event is deflected into a new $\underline{\hat{\Omega}}'$ direction of motion, but the scattered photon, which still carries the quantum of radiant energy $h(c/\lambda)$, remains in the radiation field available for eventual absorption or for a new scattering event.

Let $P(\mu', \phi')$ be the cumulative probability that photons previously moving in the $\underline{\hat{\Omega}}$ direction, are deflected into new directions at θ_0 angles from it, within the interval $(0, \theta'_0)$, and at rotation angles of rotation φ_0 around the direction $\underline{\hat{\Omega}}$, within the interval $(0, \phi')$:

$$P(\mu'_0, \phi') = \frac{1}{4\pi} \int_0^{\phi'} \mathrm{d}\phi_0 \int_{-1}^{\mu'_0} \mathrm{d}\mu_0 B(\mu_0) \tag{6}$$

From Eq. (6), it readily follows

$$\begin{aligned} P(\mu'_0, \phi') = P(\mu'_0)P(\phi') &= \left[\frac{1}{2}\int_{-1}^{\mu'_0} \mathrm{d}\mu_0 B(\mu_0)\right]\left[\frac{1}{2\pi}\int_0^{\phi'} \mathrm{d}\phi_0\right] \\ &= \left[\frac{1}{2}\int_{-1}^{\mu'_0} \mathrm{d}\mu_0 B(\mu_0)\right]\left[\frac{\phi'}{2\pi}\right] \end{aligned} \tag{7}$$

where

$$P(\mu'_0) = \left[\frac{1}{2}\int_{-1}^{\mu'_0} \mathrm{d}\mu_0 B(\mu_0)\right] \tag{8}$$

$$P(\phi') = \left[\frac{1}{2\pi}\int_0^{\phi'} \mathrm{d}\phi_0\right] = \left[\frac{\phi'}{2\pi}\right] \tag{9}$$

In this study, the phase function was expressed as a truncated Legendre polynomial expansion (39,40)

$$B(\mu_0) = 1 + \sum_{n=1}^{5} c_n P_n(\mu_0) \tag{10}$$

where

$$P_n(\mu_0) = \sum_{k=0}^{[n/2]} \left[\frac{(-1)^k (2n-2k)!}{2^n k!(n-k)!(n-2k)!}\right] \mu_0^{n-2k} \tag{11}$$

In Eq. (11), the symbol $[n/2]$ stands for the largest integer equal or less than $n/2$. Substituting Eqs. (10) and (11) in Eq. (8), the integral gives a polynomial expression in the variable μ'_0. A random number $0 \le \delta_\mu \le 1$ is obtained and assigned to $P(\mu'_0)$, thus generating an equation in the unknown μ'_0, which has to be solved numerically.

On the other hand, the φ' angle can be obtained by generating a random number $0 \le \delta_\varphi \le 1$ and then calculating $\varphi' = 2\pi(1 - \delta_\varphi)$, according to Eq. (9).

With the values of μ and φ already known from the photon direction before scattering, and with the values of μ'_0 and φ', which have been generated as described, the value of the unknown μ' can be obtained by solving the following equation

$$\mu'_0 = \left(\underline{\hat{\Omega}}' \cdot \underline{\hat{\Omega}}\right) = \left(1-\mu^2\right)^{1/2}\left(1-\mu'^2\right)^{1/2}\cos(\phi' - \phi) + \mu\mu' \tag{12}$$

thus determining completely the direction of deflection of the photon after scattering.

Monte Carlo simulation module of the direct transmittance, the diffuse reflectance and diffuse transmittance of the algal suspension: In the computational model employed to simulate the experiments, the monochromatic light beam emerging from the radiant source is assumed to be made of a large number of individual λ photons. Each photon is treated as a particle that is fired from the monochromatic light source with an initial direction $\underline{\hat{\Omega}}_0$ and impacts on the cuvette transparent wall facing the light source. At that point the photon can be either reflected or transmitted into the algal suspension. If the second possibility holds, the photon trajectory is simulated according to the strategy previously described. When the photon reaches a boundary it can be reflected toward the suspension, or can exit it. Those photons leaving the algal suspension from the cuvette wall facing the light source, in addition to those that were initially reflected on the same wall, contribute to the simulation of the diffuse reflectance. On the other hand, the photons that leave the suspension through the face opposite to the light source contribute to the direct and diffuse transmittance.

For the direct transmittance simulation, among the directions of all the photons leaving the cuvette only those that impact the detector positioned as it is schematically shown in Fig. 2a are considered. The comparison of simulation results with those of experimental measurements is based on the ratio of the computed number of photons that impact the detector to the total number of photons emitted from the light source during the same period of time.

The reflectivity $\rho_{1,2}$ on the interface between two dielectric media is computed according to Fresnell's law

$$\begin{aligned} \rho_{1,2}(\underline{\hat{\Omega}}, \underline{\hat{\Omega}}', \underline{\hat{n}}_{2,1}) = &\frac{1}{2}\left(\frac{\eta_1(\underline{\hat{n}}_{2,1} \cdot \underline{\hat{\Omega}}) - \eta_2(\underline{\hat{n}}_{2,1} \cdot \underline{\hat{\Omega}}')}{\eta_1(\underline{\hat{n}}_{2,1} \cdot \underline{\hat{\Omega}}) + \eta_2(\underline{\hat{n}}_{2,1} \cdot \underline{\hat{\Omega}}')}\right)^2 \\ &+ \frac{1}{2}\left(\frac{\eta_1(\underline{\hat{n}}_{2,1} \cdot \underline{\hat{\Omega}}') - \eta_2(\underline{\hat{n}}_{2,1} \cdot \underline{\hat{\Omega}})}{\eta_1(\underline{\hat{n}}_{2,1} \cdot \underline{\hat{\Omega}}') + \eta_2(\underline{\hat{n}}_{2,1} \cdot \underline{\hat{\Omega}})}\right)^2 \end{aligned} \tag{13}$$

where $\underline{\hat{\Omega}}$ is the direction of the beam incident on the interface from the medium 1 side; $\underline{\hat{\Omega}}'$ is the direction of the beam refracted into medium 2; $\underline{\hat{n}}_{2,1}$ is the local unit normal to the interface pointing to medium 1; and η_1 and η_2 are the refraction indices of medium 1 and medium 2, respectively. The direction $\underline{\hat{\Omega}}$ of the refracted beam is related to the direction $\underline{\hat{\Omega}}$ of the incident beam through Snell's refraction law.

After the reflectivity $\rho_{1,2}$ on the interface between dielectric media 1 and 2 has been computed, a random number $0 \le \delta_\rho \le 1$ is generated. If $0 \le \delta_\rho \le \rho_{1,2}$ then the photon is considered to be reflected and the new direction is computed according to Fresnel's reflection law. Otherwise the photon is refracted into the second media and the new direction is computed according to Snell's law.

The case of a rigid transparent material was treated as two parallel interfaces without thickness separated from one another by the wall width. The total reflectivity was computed as follows:

$$\rho_{1,2,3} = \rho_{1,2} + \left(1-\rho_{2,1}\right)\rho_{2,3}\left(1-\rho_{1,2}\right) + \rho_{1,3}\rho_{2,1}\rho_{2,3}\left(1-\rho_{1,2}\right) \tag{14}$$

where subscripts 1 and 3 denote the two media separated by the wall; subscript 2 refers to the thin transparent wall; and $\rho_{i,j}$ is the reflectivity of the (i, j) interface, computed by means of Fresnell's law, as before.

Parameter estimation: For the estimation of the scattering and absorption probabilities, as well as the parameters of the phase function, an optimization program based on a genetic algorithm was used (Fig. 5). This program provides the Monte Carlo subroutine with randomly generated sets of parameter values. Each set of values is called an "individual"; each value of the parameters given rise to an individual is expressed in the binary numerical system and is called a "gene"; and simultaneous "individuals" form together a "generation." The Monte Carlo subroutine is run for each "individual" of the

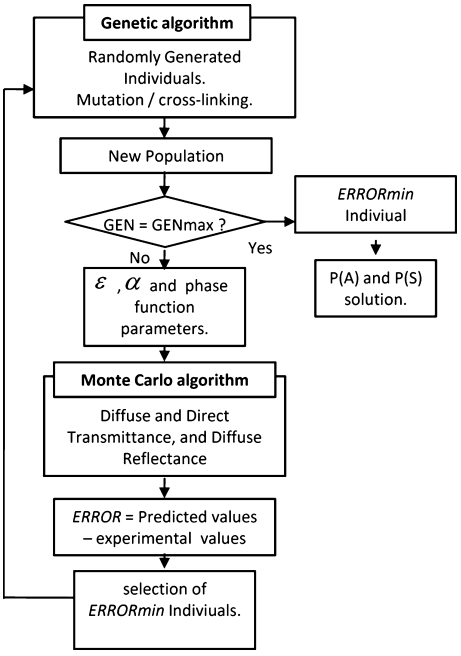

Figure 5. Schematic representation of the Genetic Algorithm–Monte Carlo Simulation Module ensemble used for the regression of the absorption and scattering spectral volumetric coefficients, and of the scattering phase function parameters.

current generation and computes an error between predicted and experimental values. The ''fittest'' individual of a generation is that which causes the least error compared to those of the other trial individuals. This individual is spared for the next generation. The other individuals of a generation are obtained by simple operations on the genes: ''mutations'' and ''hybridization.'' The procedure is repeated until an individual causes the error to fall below an acceptable ceiling value.

A genetic algorithm is a non deterministic optimization method of global search. In those cases in which the general features of the target function are poorly foreseeable, an optimization program based on a genetic algorithm is an excellent means to provide the solution to the system avoiding falling in local minima. This stochastic method has the advantage of avoiding often cumbersome manipulations of the mathematical model to derive expressions on which the assessment of the predicted results will be based. Furthermore, the choice of the initial conditions has a marginal effect on securing the solution to the problem (37,38).

The probability of absorption and scattering was individually optimized for each wavelength and algal species assuming a linear dependence of the absorption and scattering coefficients with the chlorophyll concentration and the algal DW concentration. The regression for the absorption α_λ and scattering ξ_λ coefficients were then computed as it was described elsewhere in the section.

RESULTS AND DISCUSSION

The availability of algorithms for the prediction of the local light density at any position in a culture medium is necessary either for the computation of the local microalgae growth kinetics or for the regression of its parameters, as well as for PBRs' design and optimization. In any case, it is essential knowing the optical properties of microalgae suspensions.

In this study, two microalgae species of quite different shapes were chosen as model microorganisms (*S. quadricauda* and *Chlorella* sp.) to experimentally confirm the soundness of the assumption that light scattering depends very weakly on the algal cell shape, considering the fact that not only the algal cell causes the dispersion of light but also its cellular contents, including a set of components differing in their number, size, shape and optical properties.

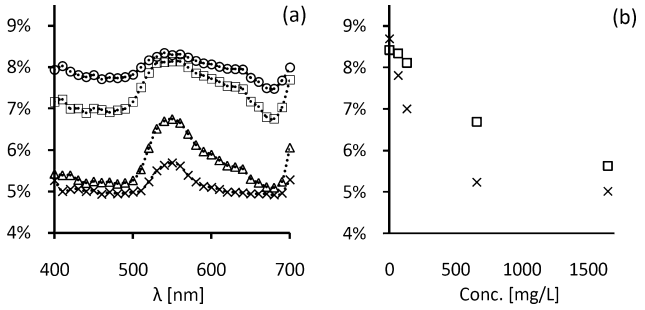

Figure 6. Relative diffuse reflectance: (a) as a function of wavelength at four different dry weight (DW) algal concentrations {1.650 g L^{-1} (×), 0.660 g L^{-1} (△), 0.132 g L^{-1} (□) and 0.066 g L^{-1} (○)}; (b) as a function of DW algal concentrations at 450 (×) and 540 nm (□) wavelengths.

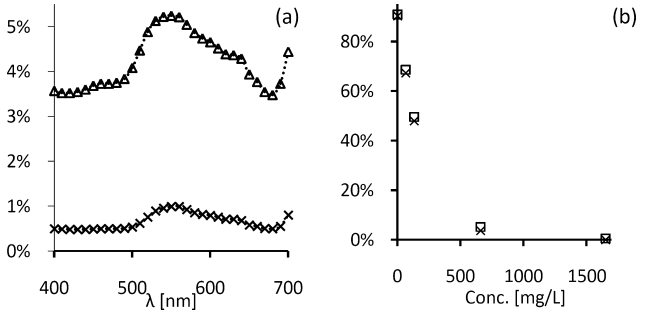

Figure 7. Relative direct transmittance: (a) as a function of wavelength at two different dry weight (DW) algal concentrations {1.650 g L^{-1} (×), 0.660 g L^{-1} (△)}; (b) as a function of DW algal concentrations for 450 (×) and 540 nm (□) wavelengths.

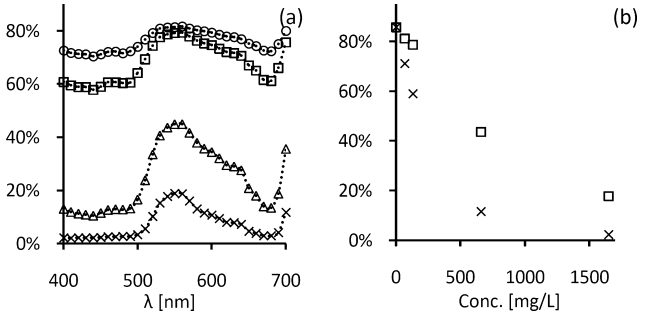

Figure 8. Relative diffuse transmittance (a) as a function of wavelength for four different dry weight (DW) algal concentrations {1.650 g L^{-1} (×), 0.660 g L^{-1} (△), 0.132 g L^{-1} (□) and 0.066 g L^{-1} (○)}; (b) as a function of DW algal concentrations for 450 (×) and 540 nm (□) wavelengths.

Measured direct transmittance, diffuse reflectance and transmittance

The results of these experiments for different suspensions of *Chlorella* sp. are shown in Figs 6–8. Although not shown for brevity, graphs of the same measurements on suspensions of *S. quadricauda* closely follow these patterns.

Figure 6a shows that the diffuse reflectance decreases as the algal DW concentration increases in the entire range of

scanned wavelengths, and that the attenuation is more important at those wavelengths where photosynthetic absorption occurs. In Fig. 6b, it can be seen that the values of the diffuse reflectance for very low algal concentrations are close to those of the reflectance measured on the cuvette filled with distilled water, where its two opposed walls, transverse to the direction of the incident beam, contribute to the total diffuse reflectance. In the case of concentrated suspensions, the measured values of the diffuse reflectance approach those of the reflectance on the first wall encountered by the light beam.

Strong evidence can be found in the literature indicating that the scattering phase function is nonisotropic and that it favors forward scattering over backward scattering (14,20,22,23). Thus, at low biomass concentrations, where single scattering prevails, the lowering trend of the diffuse reflectance with the biomass concentration is an expected result, due to the increasing energy absorption by photosynthetic pigments along the way of the photons toward the second cuvette wall, and backward after they have been reflected on it. In the case of concentrated suspensions, the measured values of the diffuse reflectance approach those of the reflectance on the first wall of the container. This is so because the contribution to the diffuse reflectance from photons undergoing multiple scattering events until they move backward, which increases with the biomass DW concentration, competes against a simultaneously larger probability of photon absorption, giving rise to the observed decreasing trend of the diffuse reflectance with algal DW concentration.

The direct transmittance decays with the DW algal concentration in an exponential-like fashion, as shown in Fig. 7b. Direct transmittance shows wavelength dependence over the entire concentration range. The difference between direct transmittances at photosynthetic and nonphotosynthetic wavelengths becomes smaller as the biomass concentration increases. At low concentrations the difference is mainly due to absorption, but with increasing biomass concentration this difference becomes smaller due to the fact that scattering becomes the dominant phenomenon (Fig. 7a). Light scattering reduces the ratio of recorded energy to incident energy as the algal concentration increases, thus progressively smoothing the dependence of the direct transmitted spectrum with wavelength due to selective absorption.

The diffuse transmittance decreases steadily with the algal mass concentration, but this trend is clearly dependent on the wavelength of the incident radiation, as shown in Figs 8a–b. As it can be expected, energy beam attenuation by absorption is more pronounced at photosynthetically active wavelengths. As in the case of direct transmittance measurements, the light rays coming out of the suspension are scattered into many directions. The difference is that in the case of diffuse transmittance experiments, light scattering has virtually no effect on the ratio of recorded energy to incident energy as the algal concentration increases, thus enhancing the wavelength dependence of the transmitted spectrum due to highly selective light absorption.

In this study, our aim is developing a simulation method for the prediction and optimization of the radiation field in PBRs and for that end, it is essential knowing the radiation field parameters governing the interaction of radiative energy with microalgae suspensions. Having capabilities to predict the local specific rate of energy absorption is particularly important when proposing algal growth kinetic expressions based on mechanisms that depend on the energy density in the expression of the rate of their initial step (41). The selectivity on wavelength of the light absorption by the photosynthetic system of green algae, which uses the radiation included in the ranges of 400–500 nm and 620–690 nm, led us to compute the local density of radiant energy for wavelengths within these ranges, as they are the ones of major interest in growth kinetics.

Table 2. "Best fit" set of optical parameters at 450 nm for the reference suspension of *Chlorella* sp.

Parameter	Value
C_1	2.496
C_2	2.852
C_3	2.173
C_4	1.107
C_5	0.302
ξ^0_{450}	0.552
α^0_{450}	0.276

Regression of the scattering and absorption coefficients from experimental data. Selection of the scattering phase function and assessment of the parameters involved

The optimization program supplies the Monte Carlo simulation subprogram with provisional values of the scattering and absorption coefficients as well as those of the parameters of the phase function, and it returns the corresponding value of the error function to the main genetic algorithmic program, which minimizes the differences between the experimental data with those predicted by the stochastic model.

Different bibliographic sources point out that the phase function for scattering in microalgal suspensions can be modeled using the Henyey–Greenstein phase function (14,20,22,23). The performance of the Henyey–Greenstein model for the prediction of the outcome of the experimental measurements was tried, but these were not reproduced with acceptable accuracy. Instead, we followed the strategy used by Chu and Churchill (42). The scattering phase function was expanded in a series of Legendre polynomials as functions of the cosine of the scattering angle, whose convergence to the correct function at any point in the interval $-1 < \mu_0 = \underline{\hat{\Omega}}' \cdot \underline{\hat{\Omega}} < 1$ is guaranteed if a sufficient number of numerically meaningful terms are included. As we shall see later on, a truncated expansion including six terms (*i.e.* that includes five parameters to be regressed. See Eqs. [10] and [11]) suffices to reproduce the experimental measurements with great accuracy.

The "best fit" parameter set obtained with the truncated Legendre expansion approximation of the scattering phase function for the reference suspension of *Chlorella sp* at 450 nm is given in Table 2, together with the values for the scattering and absorption coefficient for the most concentrated suspension at the same wavelength. In Fig. 9a, the shape of the phase function is shown.

The scattering and absorption coefficients and the parameters for the Legendre expansion were obtained at every 10 nm, in the wavelengths region from 400 to 700 nm. The

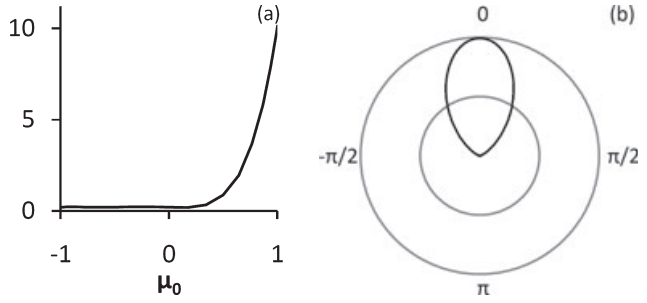

Figure 9. Phase function for the five-parameter truncated Legendre polynomial expansion. (a) *B vs* μ_0, (b) *B vs* θ_0 in polar coordinates.

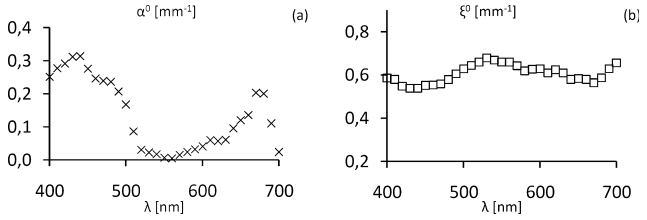

Figure 10. α_λ^0 coefficients of absorption *vs* wavelength (a) and ξ_λ^0 coefficients of scattering *vs* wavelength (b) within the 400–700 nm region for the 1.65 g L^{-1} *Chlorella* sp. suspension.

variation of the absorption coefficient shows the expected result, presenting the larger values at those wavelengths where the chlorophyll pigments are active to light (see Fig. 10a). Free chlorophylls show strong absorption peaks around 435 and 676 nm (Chlorophyll *a*) and around 475 and 650 nm (Chlorophyll *b*; 43). These peaks are not observed in the experimental transmittance measurements on algal suspensions, where chlorophylls are bound to their supporting proteins, and their absorption peaks shift their positions with respect to those of free chlorophylls to the point that they overlap, giving rise to a smoother transmittance spectrum. For the same reason, those peaks are also smoother in the plots of the absorption coefficients *vs* wavelength.

From Fig. 11a, it can be observed that the values of the experimentally measured direct transmittance, diffuse transmittance and reflectance steadily decrease with increasing values of the monochromatic volumetric absorption coefficient describing a systematic pattern, regardless the corresponding values of the wavelength within the experimental range from 400 to 700 nm. On the other hand, when the same experimental values of these properties are plotted against increasing values of the volumetric scattering coefficient as in Fig. 11b, no definite pattern can be observed and the experimental points appear rather scattered. This is an indication that photon absorption plays an important role in determining the outcome of each of these experiments. Moreover, we could claim that these experimental results depend on wavelength mainly through the absorption coefficient. As they also depend on the values of the volumetric scattering coefficient and the phase function, the corollary is that these two properties are almost wavelength independent. Moreover, the results shown in Fig. 10b corroborate this assertion for the case of the volumetric scattering coefficient.

The trapping of light energy is the key to photosynthesis. The first event is the absorption of light by the photoreceptor molecule. The principal photoreceptor in the chloroplasts of

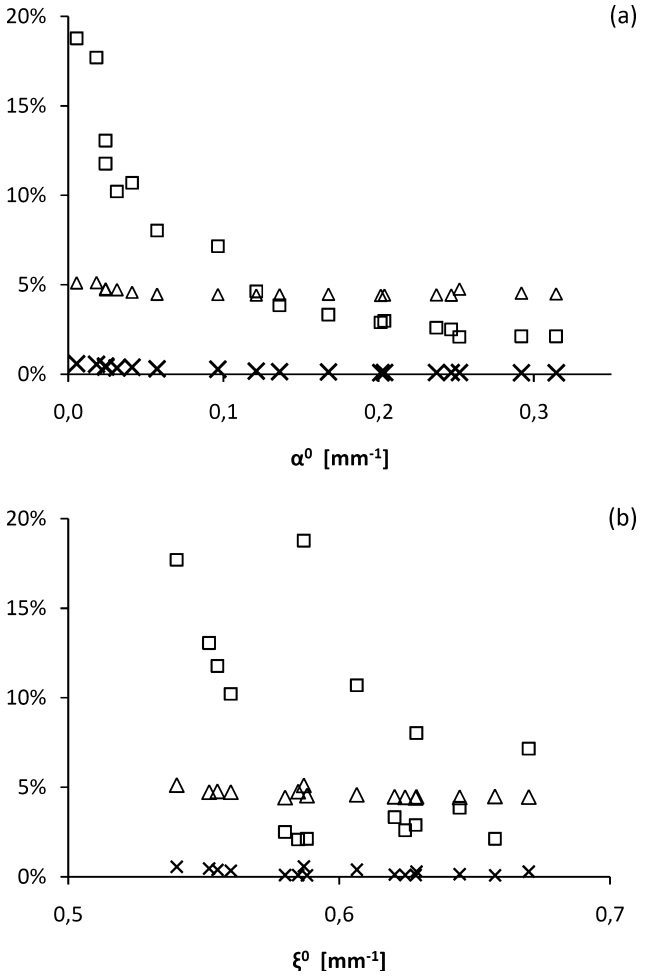

Figure 11. Relative direct transmittance (△), relative diffuse transmittance (□) and relative diffuse reflectance (×) as a function of coefficients of absorption α_λ^0 and as a function of coefficients of scattering ξ_λ^0.

most plants and microalgae is chlorophyll *a*. Light must cross the cellular membrane to reach the chlorophylls' molecules. Microalgae also contain a collection of particles and organelles (proteins, ribosomes, vesicles, liposomes, plastids, etc.) with different sizes, shapes and different optical properties. In Table 3, a short but illustrative list of cellular components is detailed together with their typical size parameters computed according to Özisik (43).

The difficulty of proposing rigorous theoretical approaches for the interpretation of experimental results at a microscopic level that incorporate all the variables involved in a manageable way, brings about the need to make arguable simplifying assumptions regarding the scattering centers. In particular, when microalgae cells are simplified into equal size spherical particles, and considered as if they were made of homogeneous materials of uniform physical properties, and it is assumed that they are the actual centers of light scattering, the effects of the differences in size of the actual intracellular scattering particles are neglected and the influence of the nonhomogeneous refractive index is ignored.

Instead, we propose a simple physical model of the radiative field interaction with algae suspensions. The proposed model lies on the assumption that the algal suspension

Table 3. Sizes and approximate size factors of some cellular components.

Cellular component	Average diameter (D)† (μm)	Approximate size factor*	
		λ = 400 nm	λ = 700 nm
Mitochondria	0.5	3.9	2.2
Chloroplast	5	39.3	22.4
Nucleus	3–10	23.6–78.5	13.5–44.9
Lysosome	0.5	3.9	2.2
Ribosome	30	0.235	0.134
Typical globular protein	5	0.039	0.022

*Size factor = $\pi \cdot D/\lambda$; †taken from Alberts *et al.* [44].

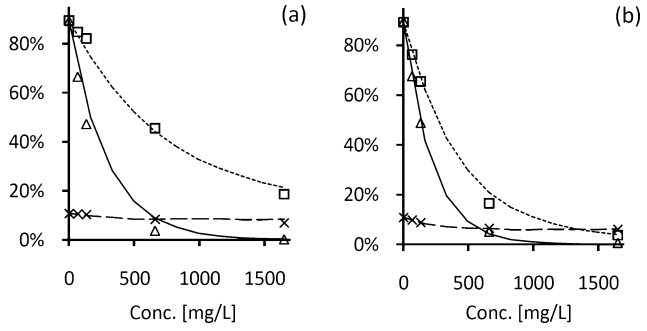

Figure 12. Direct transmittance (△,—), diffuse reflectance (×,– –) and diffuse transmittance (□,...) experimental (dots) and modeled (lines) results at 540 (a) and 450 nm (b), relative to those of the algae-free culture medium; for *Chlorella* sp. suspensions. The model parameters are: $\xi^0_{540} = 0.671\,\mathrm{mm}^{-1}$; $\xi^0_{450} = 0.552\,\mathrm{mm}^{-1}$; $\alpha^0_{540\mathrm{nm}} = 0.024\,\mathrm{mm}^{-1}$and $\alpha^0_{450\,\mathrm{nm}} = 0.292\,\mathrm{mm}^{-1}$.

can be modeled as a continuum where the actual particles that cause light scattering have been replaced with centers of absorption or scattering, randomly distributed throughout the suspension. In order that a Monte Carlo algorithm could be developed based on this model, probabilities must be assigned to the photon scattering event and to the photon absorption events, respectively, which may occur along an elementary distance travelled by the photons through the suspension (see Appendix). The experimental measurements were simulated with the Monte Carlo algorithm, using the scattering and absorption coefficients previously obtained, and with a representative set of parameters for the Legendre polynomials' expansion of the phase function (values presented in Table 2).

Experimental and predicted values of the direct transmittance, the diffuse reflectance and transmittance of the reference *Chlorella* sp. suspension using the set of coefficients of Table 2 are shown in Fig. 12a,b. This approximation to the phase function shows a good agreement with experimental data.

The light energy harvested by the photosynthetic systems is confined to the wavelength intervals from 400 to 500 nm and from 620 to 690 nm of the spectrum, and absorption within these ranges is mainly mediated by chlorophyll pigments. Carotenoids and phycobilins (in cyanobacteria and red algae) are accessory pigments and protect cells against excess irradiance. Some pigments in algae do not transfer excitation energy and some are overproduced when grown under unfavorable conditions (*i.e.* nutrient deficiency, temperature extremes and high irradiance; 45). The last conditions are not usually found in microalgae biomass production in PBRs. Considering that the chlorophyll content of the algal cells depends on the conditions of the culture process, we will correlate the spectral volumetric absorption coefficient with the concentration of chlorophyll in the algal suspension rather than with the algal DW concentration. The following linear relationships were proposed to correlate the results from the set of four different suspensions of *Chlorella* sp. prepared as described previously by dilution of the reference suspensions of Table 1:

$$\xi_\lambda\left[\frac{1}{\mathrm{mm}}\right] = \xi_\lambda^{\mathrm{DW}}\left[\frac{\mathrm{L}}{\mathrm{mg\,mm}}\right] x\left[\frac{\mathrm{mg}}{\mathrm{L}}\right] \tag{15}$$

$$\alpha_\lambda\left[\frac{1}{\mathrm{mm}}\right] = \alpha_\lambda^{\mathrm{Chl}}\left[\frac{\mathrm{L}}{\mathrm{mg\,mm}}\right] \mathrm{Chl}\left[\frac{\mathrm{mg}}{\mathrm{L}}\right] \tag{16}$$

where $\xi_\lambda^{\mathrm{DW}}$ is the specific scattering coefficient referred to unit DW algal concentration and $\alpha_\lambda^{\mathrm{Chl}}$ is the specific absorption coefficient referred to unit Chlorophyll concentration.

For the validation of our assertion regarding that: (1) the shape and size of the microalgae cells have a minor effect on the scattering coefficient and on the scattering phase function; (2) the scattering coefficient is proportional to the microalgae DW concentration (independently of the algal species); and (3) the absorption coefficient, at those wavelengths where chlorophylls are the principal absorption pigments, is proportional to the chlorophylls total concentration, we proceeded as follows. Using the set of coefficients of the expansion of the phase function in terms of Legendre polynomials; the specific scattering coefficient $\xi_\lambda^{\mathrm{DW}}$ and the specific absorption coefficient $\alpha_\lambda^{\mathrm{Chl}}$, all obtained for *Chlorella* sp. suspensions, we simulated the outcome of the experimental measurements on *S. quadricauda* suspensions and compare the measured data with the simulation results.

In Fig. 13, the experimental values of the spectral direct transmittance, the spectral diffuse transmittance and the spectral diffuse reflectance, all measured on suspensions of *S. quadricauda* at three different wavelengths, are plotted together with the corresponding values predicted by the Monte Carlo simulation algorithm using the optical parameters obtained with the same experiments performed on suspensions of *Chlorella* sp., of quite different shape compared with that of *S. quadricauda*, and also of different chlorophylls' content. As it can be seen, the simulation method predicts the experimental values with good accuracy.

CONCLUSIONS

In the present study, two important results are derived, a computer simulation tool and the optical parameters of microalgae suspensions relevant for PBRs' design and optimization purposes. The methodology proposed for the simulation of the radiation field in algae suspensions was coupled to an optimization algorithm for the assessment of the optical parameters of *Chlorella* sp. suspensions. The scattering coefficient was correlated with the algal mass concentration and the absorption coefficient was correlated with the chlorophyll concentration. The coefficients of the truncated expansion of the scattering phase function in terms

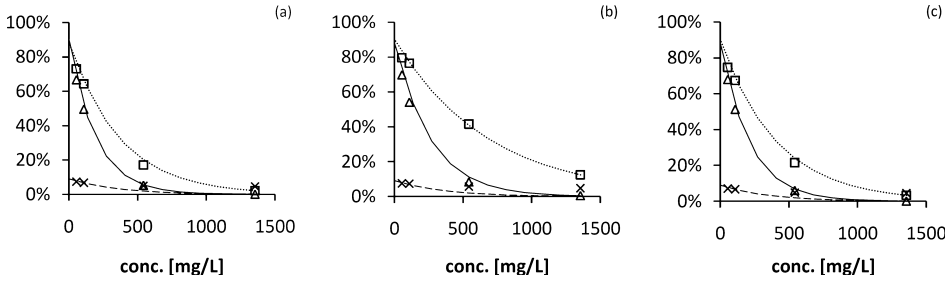

Figure 13. Direct transmittance (△,—), diffuse reflectance (×,– –) and diffuse transmittance (□,...) experimental (dots) and modeled (lines) results at 450 (a), 620 (b) and 680 nm (c), relative to those of the algae-free culture medium; for *Scenedesmus quadricauda* suspensions. The model parameters are: $\alpha_{450\ nm} = 3.5310^{-3}\ mm^{-1}$ and $\xi_{450\ nm} = 0.335\ mm^{-1}$; $\alpha_{620\ nm} = 7.3010^{-4}\ mm^{-1}$ and $\xi_{620\ nm} = 0.378\ mm^{-1}$; $\alpha_{680\ nm} = 2.5710^{-3}\ mm^{-1}$ and $\xi_{680\ nm} = 0.356\ mm^{-1}$.

of Legendre polynomials remain practically unchanged in the region from 400 to 700 nm.

When used as an autonomous simulation program the Monte Carlo module, fed with the optical coefficients regressed in the present study, permits calculating the local monochromatic energy density at any position in the algal suspension, which is crucial for the assessment of the local specific rate of monochromatic energy absorption.

Biomass productivity in any culture system depends on the degree to which the culture conditions match the requirements of the selected microorganism. Because mineral nutrient limitation is easily avoided in microalgal mass culture, availability of light inside the PBR and temperature are the main factors that determine productivity. Once the temperature is suitably controlled, light availability becomes the key limiting factor. In an optimal system where no other limiting factors are present, light availability determines the rate of photosynthesis. However, excessive light can be harmful and it is known to produce a photoinhibitory response. The central issue involved in large-scale production of photoautotrophic microalgae concerns efficient use of light for photosynthetic productivity of biomass and secondary metabolites. In addition to a mathematical model of the momentum and mass transfer in the culture media, rigorous PBR design must include a model of the radiation field, which in turn is a function of the algal mass concentration, as well as the expression of the intrinsic growth kinetic, which also depends on the local light density.

In this study, the physical model and the Monte Carlo algorithm were successfully used for simulation purposes to reproduce the experimental direct transmittance, diffuse reflectance and transmittance measured on suspensions of *S. quadricauda* (a strain with different shape and aggregation tendency), using the set of coefficients of the truncated Legendre polynomial expansion of the phase function, the specific scattering coefficient and the specific absorption coefficients obtained for *Chlorella* sp., thus implying an assurance regarding its validity. A more conclusive validation is made in a forthcoming study, for a situation closer to those found at production scales, where a polychromatic light source irradiating algal suspensions in a shallow container from its base is used, and the angular deflection of the rays and their energy is measured at different angles from the normal of the suspension free surface as they leave the suspension. This experiment can be thought of as reproducing the situation prevailing in an open pond, except that it was turned upside down for experimental convenience (46).

Acknowledgements—This work was supported by the Universidad Nacional del Litoral, CAI + D Redes N°9 "Reactores y Procesos Biológicos para la Producción de Microorganismos Sustitutos de Agroquímicos y para la Obtención de Materias Primas Alternativas para la Fabricación de Biocombustibles" and Consejo Nacional de Investigaciones Científicas y Técnicas de la República Argentina (CONICET) PIP IU "Modelado y optimización de foto-bioreactors destinados al cultivo de microorganismos fototróficos para diferentes aplicaciones biotecnológicas." The authors are grateful to Ms. G. de los Milagros Appendino and Emilio Saita for their generous contribution in part of the experimental work and to Mr. Ramón A. Saavedra and Mr. Antonio Negro for the technical support provided.

APPENDIX

Monte Carlo simulation of the radiant field in a homogeneous algal suspension

In this model, we emphasize the particle aspect rather than the wave characteristics of the radiant energy. The picture of the radiant field will be that of a nonuniform gas of photons moving in varying directions at each point with a unique speed c (*i.e.* the speed of light). Moreover, we are going to assume that in all cases of interest, the properties of the radiant energy field do not depend on time as an independent variable, but only through the time evolution of the phenomenological parameters of the radiant field which might depend, for instance, on the instantaneous composition of the background suspension. As a consequence of this, the radiant energy field will follow the changes with time of the properties of the background medium going through a succession of steady states without detectable delay.

Let's consider a thought experiment, which consists of picking a photon at a given time among those in a differential volume at the position $\underline{r}$ within the radiant energy field and keep record of its energy (*i.e.* of its wavelength λ) and of its direction of motion $\hat{\underline{\Omega}}$. If we assume that all photons are equally accessible to the observer, the sampling is not biased and the fraction of photons that move with directions enclosed by the elementary solid angle $d^{(2)}\hat{\underline{\Omega}} = \sin\theta d\theta d\phi = -d\mu d\phi$ and have wavelength between λ and $\lambda + d\lambda$ (*i.e.* the fraction of

$(\hat{\underline{\Omega}}, \lambda)$ photons among all photons around $\underline{r}$) can be regarded as the *differential probability* $\mathrm{d}^{(3)}P(\underline{r}, \hat{\underline{\Omega}}, \lambda)$of occurrence of the $(\underline{r}, \hat{\underline{\Omega}}, \lambda)$ event.

The differential probability of this compound event can be written in terms of the *probability distribution function*

$$\begin{aligned} \mathrm{d}^{(3)}P\left(\underline{r}, \hat{\underline{\Omega}}, \lambda\right) &= \frac{\partial^{(3)}}{\partial^{(2)}\hat{\underline{\Omega}}\,\partial\lambda} P\left(\underline{r}, \hat{\underline{\Omega}}, \lambda\right) \mathrm{d}^{(2)}\hat{\underline{\Omega}}\,\mathrm{d}\lambda \\ &= p\left(\underline{r}, \hat{\underline{\Omega}}, \lambda\right) \mathrm{d}^{(2)}\hat{\underline{\Omega}}\,\mathrm{d}\lambda \end{aligned} \tag{17}$$

where

$$p\left(\underline{r}, \hat{\underline{\Omega}}, \lambda\right) = \frac{\partial^{(3)}}{\partial^{(2)}\hat{\underline{\Omega}}\,\partial\lambda} P\left(\underline{r}, \hat{\underline{\Omega}}, \lambda\right) \tag{18}$$

is the probability distribution function of the $(\underline{r}, \hat{\underline{\Omega}}, \lambda)$ event.

As it is frequently carried out in the field of the kinetic theory of fluids, we require that the cumulative probability $P(\underline{r}, \hat{\underline{\Omega}}, \lambda)$ satisfies the normalization condition:

$$\begin{aligned} \int_{\lambda} \mathrm{d}\lambda \int_{\hat{\underline{\Omega}}} \mathrm{d}^{(3)}P\left(\underline{r}, \hat{\underline{\Omega}}, \lambda\right) &= \int_{\lambda} \mathrm{d}\lambda \int_{\hat{\underline{\Omega}}} \mathrm{d}^{(2)}\hat{\underline{\Omega}}\, p\left(\underline{r}, \hat{\underline{\Omega}}, \lambda\right) \\ &= \int_{\lambda} \mathrm{d}\lambda \int_{0}^{2\pi} \mathrm{d}\phi \int_{-1}^{1} \mathrm{d}\mu\, p(\underline{r}, \mu, \phi, \lambda) = n_{\mathrm{p}}(\underline{r}) \end{aligned} \tag{19}$$

where $n_{\mathrm{p}}(\underline{r})$ is the photon number density regardless of their individual direction of motion and of the wavelength they have. As a consequence of this normalization condition, we can think of $p(\underline{r}, \hat{\underline{\Omega}}, \lambda)$ as the number density $n_{\mathrm{p}}(\underline{r}, \hat{\underline{\Omega}}, \lambda)$ of λ photons around the field point $\underline{r}$ (Fig. 14), which move in the direction $\hat{\underline{\Omega}}(\mu, \phi)$. Then we can write

$$\mathrm{d}^{(3)}P\left(\underline{r}, \hat{\underline{\Omega}}, \lambda\right) = n_{\mathrm{p}}\left(\underline{r}, \hat{\underline{\Omega}}, \lambda\right) \mathrm{d}^{(2)}\hat{\underline{\Omega}}\,\mathrm{d}\lambda \tag{20}$$

For strictly computational purposes we will proceed as if we were able to keep a detailed account of the series of events that may occur to a tagged photon among those in the $n_{\mathrm{p}}(\underline{r}, \hat{\underline{\Omega}}, \lambda)$ subset, while it covers a distance Δs in its direction of motion $\hat{\underline{\Omega}}$. Along this elemental step from the field point $\underline{r}$ toward the point $\underline{r} + \hat{\underline{\Omega}}\,\Delta s$, the $(\hat{\underline{\Omega}}, \lambda)$ photon can be removed from this set at some intermediate point $\underline{r} + \alpha\hat{\underline{\Omega}}\,\Delta s$, $0 < \alpha < 1$, whether it is absorbed by the medium "or" deflected from its original direction $\hat{\underline{\Omega}}$. In either case, the $(\hat{\underline{\Omega}}, \lambda)$ photon will not reach the field point $\underline{r} + \hat{\underline{\Omega}}\,\Delta s$. Therefore, the $(\hat{\underline{\Omega}}, \lambda)$ photon can undergo only one of the following complementary, and mutually exclusive, events:

- Absorption event (A).
- Scattering event (S).
- Neither absorption nor scattering *compound* event (NA, NS).

Because these are complementary and mutually exclusive events, their probabilities of occurrence must add to unity:

$$P(\mathrm{A}) + P(\mathrm{S}) + P(\mathrm{NA,\ NS}) = 1 \tag{21}$$

The problem to address now is that of assigning a mathematical expression to each of the probabilities included in Eq. (21).

Let us consider the s coordinate along the direction of propagation $\hat{\underline{\Omega}}$ of a monochromatic radiant energy beam through an absorbing and scattering medium. Let us also consider an elementary right circular cylinder positioned around the direction $\hat{\underline{\Omega}}$ with base $\Delta\mathrm{A}$ and height Δs as sketched in Fig. 15. The *monochromatic radiant energy* due to $(\hat{\underline{\Omega}}, \lambda)$ photons entering the elemental cylinder through its virtual base at s per unit time is:

$$\begin{aligned} \Delta\dot{E}\left(s, \hat{\underline{\Omega}}, \lambda\right) &= c\, h\left(\frac{c}{\lambda}\right) n_{\mathrm{p}}\left(s, \hat{\underline{\Omega}}, \lambda\right) \Delta A\, \Delta\hat{\underline{\Omega}}\, \Delta\lambda \\ &= c\, h\nu\, n_{\mathrm{p}}\left(s, \hat{\underline{\Omega}}, \lambda\right) \Delta A\, \Delta\hat{\underline{\Omega}}\, \Delta\lambda \end{aligned} \tag{22}$$

The *monochromatic radiant energy* due to $(\hat{\underline{\Omega}}, \lambda)$ photons leaving the elementary right cylinder through its virtual base at $s + \Delta s$ per unit time, is

$$\Delta\dot{E}\left(s + \Delta s, \hat{\underline{\Omega}}, \lambda\right) = c\, h\left(\frac{c}{\lambda}\right) n_{\mathrm{p}}\left(s + \Delta s, \hat{\underline{\Omega}}, \lambda\right) \Delta A\, \Delta\hat{\underline{\Omega}}\, \Delta\lambda \tag{23}$$

Let us denote by $\Delta\dot{E}_{\mathrm{abs}}(s + \alpha\,\Delta s, \hat{\underline{\Omega}}, \lambda)$, $0 < \alpha < 1$, the radiant energy locally absorbed per unit time by the medium while $(\hat{\underline{\Omega}}, \lambda)$ photons cover the distance from s to $s + \Delta s$. A radiant energy balance performed on the elemental cylinder leads to

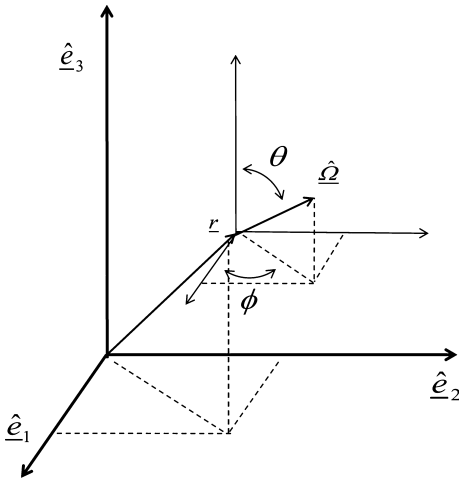

Figure 14. Unit vector $\hat{\underline{\Omega}}$ pointing in a generic direction (θ, φ) from a field point $\underline{r}$.

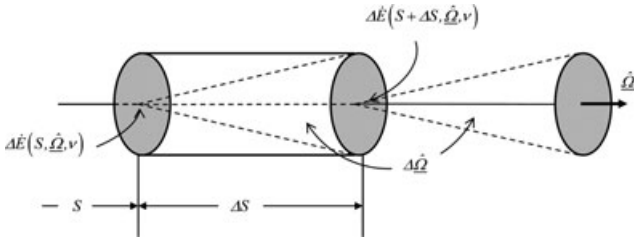

Figure 15. Radiant energy balance along an elementary beam propagation step Δs in the $\hat{\underline{\Omega}}$ direction: a supporting sketch.

$$\Delta\dot{E}\left(s,\hat{\underline{\Omega}},\lambda\right)=\Delta\dot{E}\left(s+\Delta s,\hat{\underline{\Omega}},\lambda\right)+\Delta\dot{E}_{\mathrm{abs}}\left(s+\alpha\,\Delta s,\hat{\underline{\Omega}},\lambda\right)+\Delta\dot{E}_{\mathrm{scatt}}\left(s+\alpha\,\Delta s,\hat{\underline{\Omega}},\lambda\right) \tag{24}$$

The following constitutive equations are proposed for the local volumetric rate of radiant energy absorption and for the local volumetric rate of radiant energy scattering:

$$\Delta\dot{E}_{\mathrm{abs}}\left(s+\alpha\,\Delta s,\hat{\underline{\Omega}},\lambda\right)=\alpha_\lambda c\,h\left(\frac{c}{\lambda}\right)n_{\mathrm{p}}\left(s+\alpha\,\Delta s,\hat{\underline{\Omega}},\lambda\right)\Delta s\,\Delta A\,\Delta\hat{\underline{\Omega}}\,\Delta\lambda \tag{25}$$

$$\Delta\dot{E}_{\mathrm{scatt}}\left(s+\alpha\,\Delta s,\hat{\underline{\Omega}},\lambda\right)=\xi_\lambda c\,h\left(\frac{c}{\lambda}\right)n_{\mathrm{p}}\left(s+\alpha\,\Delta s,\hat{\underline{\Omega}},\lambda\right)\Delta s\,\Delta A\,\Delta\hat{\underline{\Omega}}\,\Delta\lambda \tag{26}$$

where α_λ and ξ_λ are the *volumetric spectral absorption coefficient* and the *volumetric spectral scattering coefficient*, respectively, of the background suspension.

Substitution of Eqs. (22), (23), (25) and (26) in Eq. (24), after some obvious cancellations, gives

$$n_{\mathrm{p}}\left(s,\hat{\underline{\Omega}},\lambda\right)=n_{\mathrm{p}}\left(s+\Delta s,\hat{\underline{\Omega}},\lambda\right)+(\alpha_\lambda+\xi_\lambda)\,n_{\mathrm{p}}\left(s+\alpha\,\Delta s,\hat{\underline{\Omega}},\lambda\right)\Delta s \tag{27}$$

Equation (17) can be cast into the following form

$$\frac{1}{n_{\mathrm{p}}\left(s+\alpha\,\Delta s,\hat{\underline{\Omega}},\lambda\right)}\left[\frac{n_{\mathrm{p}}\left(s+\Delta s,\hat{\underline{\Omega}},\lambda\right)-n_{\mathrm{p}}\left(s,\hat{\underline{\Omega}},\lambda\right)}{\Delta s}\right]=-(\alpha_\lambda+\xi_\lambda) \tag{28}$$

for $\hat{\underline{\Omega}}$, $\lambda=\mathrm{const.}$ In the limit of $\Delta s\ \rightarrow\ 0$, we get

$$\frac{1}{n_{\mathrm{p}}\left(s,\hat{\underline{\Omega}},\lambda\right)}\left[\frac{\partial n_{\mathrm{p}}\left(s,\hat{\underline{\Omega}},\lambda\right)}{\partial s}\right]=-(\alpha_\lambda+\xi_\lambda) \tag{29}$$

Integration of Eq. (29) over a distance Δs along the straight trajectory $\underline{r}(s+\Delta s)=\underline{r}(s)+\hat{\underline{\Omega}}\,\Delta s$ across the homogeneous suspension, gives

$$\ln\left[\frac{n_{\mathrm{p}}\left(s+\Delta s,\hat{\underline{\Omega}},\lambda\right)}{n_{\mathrm{p}}\left(s,\hat{\underline{\Omega}},\lambda\right)}\right]=-(\alpha_\lambda+\xi_\lambda)\Delta s \tag{30}$$

$$\left[\frac{n_{\mathrm{p}}\left(s+\Delta s,\hat{\underline{\Omega}},\lambda\right)}{n_{\mathrm{p}}\left(s,\hat{\underline{\Omega}},\lambda\right)}\right]=\exp\{-(\alpha_\lambda+\xi_\lambda)\Delta s\} \tag{31}$$

In Eq. (31), the ratio $n_{\mathrm{p}}(s+\Delta s,\hat{\underline{\Omega}},\lambda)\big/n_{\mathrm{p}}(s,\hat{\underline{\Omega}},\lambda)$ is the *conditional probability* that a $(\hat{\underline{\Omega}},\lambda)$ photon reaches the position $s+\Delta s$ with $\hat{\underline{\Omega}}$ direction given the fact that it comes from the position s. This is equivalent to saying that a $(\hat{\underline{\Omega}},\lambda)$ photon that was fired from the position $\underline{r}(s,\hat{\underline{\Omega}})$ with direction $\hat{\underline{\Omega}}$ has the probability

$$P(\mathrm{NA,\ NS})=\exp\{-(\alpha_\lambda+\xi_\lambda)\Delta s\} \tag{32}$$

of reaching the position $\underline{r}(s+\Delta s)=\underline{r}(s)+\hat{\underline{\Omega}}\,\Delta s$ in a scattering and absorbing medium (*i.e.* the *probability of surviving to absorption and scattering as a*$(\hat{\underline{\Omega}},\lambda)$ *photon*).

From the Eq. (21), and taking into account the mutually exclusive character of a single photon scattering and absorption events, we conclude that the *probability of absorption or scattering* of a $(\hat{\underline{\Omega}},\lambda)$ photon fired from the position $\underline{\mathrm{r}}(s)$ after traveling a small distance Δs in the $\hat{\underline{\Omega}}$ direction through the algal suspension is

$$P(\mathrm{A''or''S})=P(\mathrm{A})+P(\mathrm{S})=1-\exp[-(\alpha_\lambda+\xi_\lambda)\Delta s] \tag{33}$$

From Eq. (25), we can see that the contribution of photon absorption to the local decrease of $(\hat{\underline{\Omega}},\lambda)$ photon number density at any intermediate point s' over the straight trajectory $\underline{r}(s+\Delta s)=\underline{r}(s)+\hat{\underline{\Omega}}\,\Delta s$ in a homogeneous medium is

$$\frac{1}{n_{\mathrm{p}}\left(s,\hat{\underline{\Omega}},\lambda\right)}\left[\frac{\partial n_{\mathrm{p}}\left(s,\hat{\underline{\Omega}},\lambda\right)}{\partial s}\right]=-\frac{1}{n_{\mathrm{p}}\left(s,\hat{\underline{\Omega}},\lambda\right)}\left[\frac{\partial n_{\mathrm{p}}^{(\mathrm{abs})}\left(s,\hat{\underline{\Omega}},\lambda\right)}{\partial s}\right]=-\alpha_\lambda \tag{34}$$

for constant $\hat{\underline{\Omega}}$ and λ.

From Eq. (25), around a position s', $s<s'<s+\Delta s$, we have

$$\begin{aligned}\mathrm{d}n_{\mathrm{p}}^{(\mathrm{abs})}\left(s',\hat{\underline{\Omega}},\lambda\right)&=-\alpha_\lambda\,n_{\mathrm{p}}\left(s',\hat{\underline{\Omega}},\lambda\right)\mathrm{d}s'\\&=-\alpha_\lambda\,n_{\mathrm{p}}\left(s,\hat{\underline{\Omega}},\lambda\right)\exp[-(\alpha_\lambda+\xi_\lambda)(s'-s)]\mathrm{d}s'\end{aligned} \tag{35}$$

Integration of Eq. (35) over the interval $s<s'<s+\Delta s$, gives

$$\begin{aligned}n_{\mathrm{p}}^{(\mathrm{abs})}\left(s+\Delta s,\hat{\underline{\Omega}},\lambda\right)&=\alpha_\lambda\,n_{\mathrm{p}}\left(s,\hat{\underline{\Omega}},\lambda\right)\int_0^{s+\Delta s}\mathrm{d}s'\exp[-(\alpha_\lambda+\xi_\lambda)(s'-s)]\\&=\frac{\alpha_\lambda}{(\alpha_\lambda+\xi_\lambda)}n_{\mathrm{p}}\left(s,\hat{\underline{\Omega}},\lambda\right)\{1-\exp[-(\alpha_\lambda+\xi_\lambda)\Delta s]\}\end{aligned} \tag{36}$$

by rearranging Eq. (36), we get

$$P(\mathrm{A})=\frac{n_{\mathrm{p}}^{(\mathrm{abs})}\left(s+\Delta s,\hat{\underline{\Omega}},\lambda\right)}{n_{\mathrm{p}}\left(s,\hat{\underline{\Omega}},\lambda\right)}=\frac{\alpha_\lambda}{(\alpha_\lambda+\xi_\lambda)}\{1-\exp[-(\alpha_\lambda+\xi_\lambda)\Delta s]\} \tag{37}$$

From Eq. (37) and the condition of Eq. (33),

$$P(\mathrm{S})=\frac{\xi_\lambda}{(\alpha_\lambda+\xi_\lambda)}\{1-\exp[-(\alpha_\lambda+\xi_\lambda)\Delta s]\} \tag{38}$$

Substitution of the expressions obtained from $P(\mathrm{A})$, $P(\mathrm{S})$, $P(\mathrm{NA,\ NS})$ in Eq. (25), gives

$$\underbrace{\frac{(\xi_\lambda)}{(\alpha_\lambda+\xi_\lambda)}\{1-\exp[-(\alpha_\lambda+\xi_\lambda)\Delta s]\}}_{P(\mathrm{S})} + \underbrace{\frac{(\alpha_\lambda)}{(\alpha_\lambda+\xi_\lambda)}\{1-\exp[-(\alpha_\lambda+\xi_\lambda)\Delta s]\}}_{P(\mathrm{A})} + \underbrace{\exp[-(\alpha_\lambda+\xi_\lambda)\Delta s]}_{P(\mathrm{S})\times P(\mathrm{A})=P(\mathrm{NS,NA})} = 1 \quad (39)$$

REFERENCES

1. Ling Xu, P. J., X. R. Weathers and C. Z. Liu Xiong (2009) Microalgal bioreactors: challenges and opportunities. *Eng. Life Sci.* **9**(3), 178–189.
2. Spolaore, P., C. Joannis-Cassan, E. Duran and A. Isambert (2006) Commercial applications of microalgae. *J. Biosci. Bioeng.* **101**(2), 87–96.
3. Borowitzka, M. A. (1992) Algal biotechnology products and processes—matching science and economics. *J. Appl. Phycol.* **4**, 267–279.
4. Kay, R. A. (1991) Microalgae as food and supplement. *Crit. Rev. Food Sci. Nutr.* **30**, 555–573.
5. Schwartz, R. E., C. F. Hirsch, D. F. Sesin, J. E. Flor, M. Chartrain and R. E. Fromtling (1990) Pharmaceuticals from cultured algae. *J. Ind. Microbiol.* **5**, 113–124.
6. Vilchez, C., I. Garbayo, M. V. Lobato and J. M. Vega (1997) Microalgae-mediated chemicals production and wastes removal. *Enzyme Microb. Technol.* **20**, 562–572.
7. Metzger, P. and C. Largeau (2005) *Botryococcus braunii*: a rich source for hydrocarbons and related ether lipids. *Appl. Microbiol. Biotechnol.* **66**, 486–496.
8. Chisti, Y. (2007) Biodiesel from microalgae. *Biotechnol. Adv.* **25**, 294–306.
9. Chisti, Y. (2008) Biodiesel from microalgae beats bioethanol. *Trends Biotechnol.* **26**, 126–131.
10. Borowitzka, M. A. (2005) Culturing microalgae in outdoor ponds. In *Algal Culturing Techniques* (Edited by R. A. Andersen), pp. 205–218. Elsevier, San Diego.
11. Behrens, P. W. (2005) Photobioreactors and fermentors: the light and dark sides of growing algae. In *Algal Culturing Techniques* (Edited by R. A. Andersen), pp. 189–204. Elsevier, San Diego.
12. Molina Grima, E., F. G. Acién Fernández, F. García Camacho and Y. Chisti (1999) Photobioreactors: light regime, mass transfer, and scaleup. *J. Biotechnol.* **70**, 231–247.
13. Rubio, F. C., F. G. Camacho, J. M. Sevilla, Y. Chisti and E. Molina Grima (2003) A mechanistic model of photosynthesis in microalgae. *Biotechnol. Bioeng.* **81**, 459–473.
14. Pilon, L., H. Berberoglu and R. Kandilian (2011) Radiation transfer in photobiological carbon dioxide fixation and fuel production by microalgae. *J. Quant. Spectrosc. Ra.* **112**(17), 2639–2660.
15. Pruvost, J., J. Legrand, P. Legentilhomme and A. Muller-Feuga (2002) Simulation of microalgae growth in limiting light conditions: flow effect. *AIChE J.* **48**(5), 1109–1120.
16. Acién Fernández, F. G., F. García Camacho, J. A. Sánchez Pérez, J. M. Fernández Sevilla and E. Molina Grima (1997) A model for light distribution and average solar irradiance inside outdoor tubular photobioreactors for the microalgal mass culture. *Biotechnol. Bioeng.* **55**(5), 701–714.
17. Cornet, J. F., C. G. Dussap and G. Dubertret (1992) A structured model for simulation of cultures of the cyanobacterium *Spirulina platensis* in photobioreactors: I. Coupling between light transfer and growth kinetics. *Biotechnol. Bioeng.* **40**(7), 817–825.
18. Cornet, J. F., C. G. Dussap, P. Cluzel and G. Dubertret (1992) A structured model for simulation of cultures of the cyanobacterium *Spirulina platensis* in photobioreactors: II. Identification of kinetic parameters under light and mineral limitations. *Biotechnol. Bioeng.* **40**(7), 826–834.
19. Cornet, J. F., C. G. Dussap, J. B. Gross, C. Binois and C. Lasseur (1995) A simplified monodimensional approach for modeling coupling between radiant light transfer and growth kinetics in photobioreactors. *Chem. Eng. Sci.* **50**(9), 1489–1500.
20. Berberoglu, H. and L. Pilon (2009) Radiation characteristics of *Botryococcus braunii*, *Chlorococcum littorale*, and *Chlorella* sp. used for CO_2 fixation and biofuel production. *J. Quant. Spectrosc. Ra.* **110**, 1879–1893.
21. Özisik, M. N. (1973) Chapter 8. In *Radiative Transfer and Interactions with Conduction and Convection* (Edited by M. N. Özisik), pp. 249–253. John Wiley & Sons, New York.
22. Berberoglu, H. and L. Pilon (2007) Experimental measurement of the radiation characteristics of *Anabaena variabilis* ATCC 29413-U and *Rhodobacter sphaeroides* ATCC 49419. *Int. J. Hydrogen Energy* **32**(18), 4772–4785.
23. Berberoglu, H., A. Melis and L. Pilon (2008) Radiation characteristics of *Chlamydomonas reinhardtii* CC125 and its truncated chlorophyll antenna transformants tla1, and tla1-CW. *Int. J. Hydrogen Energy* **33**(22), 6467–6483.
24. Pottier, L., J. Pruvost, J. Deremetz, J. F. Cornet, J. Legrand and C. G. Dussap (2005) A fully predictive model for one-dimensional light attenuation by *Chlamydomonas reinhardtii* in a torous photobioreactor. *Biotechnol. Bioeng.* **91**(56), 9–582.
25. Agrawal, B. M. and M. P. Mengüc (1991) Forward and inverse analysis of single and multiple scattering of collimated radiation in an axisymmetric system. *Int. J. Heat Mass Transfer* **34**, 633–647.
26. Bohren, C. F. and D. R Huffman (1998) *Absorption and Scattering of Light by Small Particles*, pp. 130–132. John Wiley & Sons, New York.
27. Stramski, D. and J. Piskozub (2003) Estimation of scattering error in spectro-photometric measurements of light absorption by aquatic particles from three-dimensional radiative transfer simulations. *Appl. Optics* **42**, 3634–3646.
28. Heldt, H. W. (2004) The use of energy from sunlight by photosynthesis is the basis of life on earth. In *Plant Biochemistry* (Edited by H. W. Heldt), pp. 45–66. Elsevier, San Diego.
29. Heldt, H. W. (2004) Photosynthesis is an electron transport process. In *Plant Biochemistry* (Edited by H. W. Heldt), pp. 67–114. Elsevier, San Diego.
30. Frenkel, D. (2004) Introduction to Monte Carlo methods. In *Computational Soft Matter: From Synthetic Polymers to Proteins, Lecture Notes* (Edited by N. Attig, K. Binder, H. Grubmuller and K. Kremer), pp. 29–60. John von Neumann Institute for Computing, Jülich. NIC Series, Vol. 23.
31. Csögör, Z., M. Herrenbauer, K. Schmidt and C. Posten (2001) Light distribution in a novel photobioreactor—modelling for optimization. *J. Appl. Phycol.* **13**, 325–333.
32. Rosello Sastre, R., Z. Csögör, I. Perner-Nochta, P. Fleck-Schneider and C. Posten (2007) Scale-down of microalgae cultivations in tubular photo-bioreactors—a conceptual approach. *J. Biotechnol.* **132**, 127–133.
33. Atlas, R. M. (2005) *Handbook of Media for Environmental Microbiology*, pp. 67–68. Taylor & Francis, Boca Raton.
34. Eaton, A. D., L. S. Clesceri, E. W. Rice and A. E. Greenberg (2005) *Standard methods for the examination of water and wastewater*, 21st ed. Part 10000, Biological Examination Michael K. Hein, pp. 10–26 to 10–27. American Public Health Association, Washington, DC.
35. Ritchie, R. J. (2008) Universal chlorophyll equations for estimating chlorophylls *a*, *b*, *c* and *d* and total chlorophylls in natural assemblages of photosynthetic organisms using acetone, methanol or ethanol solvents. *Photosynthetica*, **46**(1), 115–126.
36. Satuf, M. L., R. J. Brandi, A. E. Cassano and O. M. Alfano (2005) Experimental method to evaluate the optical properties of aqueous titanium dioxide suspensions. *Ind. Eng. Chem. Res.* **44**, 6643–6649.
37. Deb, K. (2001) *Multi-Objective Optimization using Evolutionary Algorithms*, pp. 84–132. Wiley, Chichester, UK.
38. Rezende, M. C. A. F., C. B. B. Costa, A. C. Costa, M. R. Wolf Maciel and R. Maciel Filho (2008) Optimization of a large scale industrial reactor by genetic algorithms. *Chem. Eng. Sci.* **63**, 330–341.
39. Lebedev, N. N. (1972) Chapter 4. In *Special Functions and their Applications* (Edited by R. A. Silverman), pp. 44–53. Dover Publications Inc., New York.
40. Hu, Y.-X., B. Wielicki, B. Lin, G. Gibson, S. C. Tsay, K. Stamnes and T. Wong (2000) Delta-Fit: a fast and accurate treatment of

particle scattering phase functions with weighted singular-value decomposition least-squares fitting. *J. Quant. Spectrosc. Radiat. Transfer* **65**, 681–690.
41. Alfano, O. M., H. A. Irazoqui and A. E. Cassano (2009) The local and observed photochemical reaction rates revisited. *Photochem. Photobiol. Sci.* **8**, 1047–1058.
42. Chu, C.-M. and S. W. Churchill (1955) Representation of the angular distribution of radiation scattered by a spherical particle. *J. Opt. Soc. Am.* **45**, 958–962.
43. Özisik, M. N. (1973) Chapter 2. In *Radiative Transfer and Interactions with Conduction and Convection* (Edited by M. N. Özisik), pp. 55–120. John Wiley & Sons, New York.
44. Alberts, B., D. Bray, J. Lewis, M. Raff, K. Roberts and J. D. Watson (1994) *Molecular Biology of the Cell*, 3rd edition, pp. 16–17. Garland Science, New York.
45. Masojidek, J., M. Koblizek and G. Torzillo (2005) Photosynthesis in microalgae. In *Handbook of Microalgal Culture: Biotechnology and Applied Phycology* (Edited by A. Richmond), pp. 23–26. Blackwell Publishing Ltd, Oxford.
46. Heinrich, J. M., F. A. Botta, I. Niizawa, A. R. Trombert and H. A. Irazoqui (2012). Analysis and design of photobioreactors for microalgae production II: experimental validation of a radiation field simulator based on a Monte Carlo algorithm. *Photochem. Photobiol.*, doi:10.1111/j.1751-1097.2012.01149.x